Available online at www.sciencedirect.com
SCIENCE DIRECT®
Astroparticle Physics xxx (2004) xxx–xxx
Astroparticle Physics
www.elsevier.com/locate/astropart

# Neutron background in large-scale xenon detectors for dark matter searches

M.J. Carson, J.C. Davies, E. Daw, R.J. Hollingworth, V.A. Kudryavtsev *, T.B. Lawson, P.K. Lightfoot, J.E. McMillan, B. Morgan, S.M. Paling, M. Robinson, N.J.C. Spooner *, D.R. Tovey

*Department of Physics and Astronomy, University of Sheffield, Hicks Building, Hounsfield Road, Sheffield S3 7RH, UK*

Received 20 November 2003; received in revised form 1 May 2004; accepted 2 May 2004

**Abstract**

Simulations of the neutron background for future large-scale particle dark matter detectors are presented. Neutrons were generated in rock and detector elements via spontaneous fission and $(\alpha, n)$ reactions, and by cosmic-ray muons. The simulation techniques and results are discussed in the context of the expected sensitivity of a generic liquid xenon dark matter detector. Methods of neutron background suppression are investigated. A sensitivity of $10^{-9}$–$10^{-10}$ pb to WIMP-nucleon interactions can be achieved by a tonne-scale detector.


*PACS:* 14.20.Dh; 14.80.Ly; 13.60.Rj; 13.75.−n; 13.85.−t; 28.20; 25.40; 98.70.Vc
*Keywords:* Dark matter; WIMPs; Neutron background; Neutron flux; Spontaneous fission; $(\alpha, n)$ reactions; Radioactivity; Cosmic-ray muons underground; Photomultipliers

## 1. Introduction

Future dark matter experiments planning to reach a sensitivity of $10^{-9}$–$10^{-10}$ pb to the WIMP-nucleon cross-section require a very low background environment, sophisticated techniques capable of discriminating WIMP-induced events from all kinds of background and at least one tonne of target mass to achieve sufficient counting rate. Hereafter, the quoted sensitivity refers to the minimum of the sensitivity curve, which occurs for WIMP masses in the range 40–80 GeV (see, for instance, Fig. 13 for examples of the sensitivity or exclusion curves). Some individual background events, however, are indistinguishable from expected WIMP scattering events. WIMPs are expected to interact with ordinary matter in detectors to produce nuclear recoils, which can be detected through ionisation, scintillation or phonons. Identical events can be induced by single elastic scattering of neutrons. Thus, only suppression of any background neutron flux by passive or active

* Corresponding authors. Tel.: +44-114-2224531; fax: +44-114-2728079.
*E-mail addresses:* v.kudryavtsev@sheffield.ac.uk (V.A. Kudryavtsev), n.spooner@sheffield.ac.uk (N.J.C. Spooner).

0927-6505/$ - see front matter © 2004 Published by Elsevier B.V.
doi:10.1016/j.astropartphys.2004.05.001

shielding and proper choice of detector materials will allow experiments to reach sufficiently high sensitivity to WIMPs. Designing detectors, their shielding and active veto systems requires simulation of neutron fluxes from various sources.

Neutrons underground arise from two sources: (i) local radioactivity, and (ii) cosmic-ray muons. Neutrons associated with local radioactivity are produced mainly via $(\alpha, n)$ reactions initiated by $\alpha$-particles from U/Th traces in the rock and detector elements. Neutrons from spontaneous fission of $^{238}$U also contribute to the flux. The neutron yield from cosmic-ray muons depends strongly on the depth of the underground laboratory. The suppression of the muon flux by a large rock overburden will also reduce the neutron flux but by a smaller factor.

In the present study neutrons associated with radioactivity in rock and detector elements are treated separately. Although these neutrons come from similar reactions, the materials in which they are produced are certainly different, as are the methods of their suppression. Neutrons from surrounding rock can be easily suppressed by passive hydrocarbon shielding, whereas the internal neutron flux can be reduced by choosing ultra-low-background materials and possibly by using an active veto to reject events in the detector in coincidence with veto signals.

At deep underground sites (3 km w.e. or more), the neutron production rate from muons is about 3 orders of magnitude lower than the rate for neutrons arising from rock activity, depending strongly both on the depth and the U/Th contamination. The muon-induced neutron flux can be important, however, for experiments intending to reach high sensitivity to WIMPs. There are several reasons for this: (1) the energy spectrum of muon-induced neutrons is hard, extending to GeV energies, and fast neutrons can travel far from the associated muon track, reaching a detector from large distances; (2) fast neutrons transfer larger energies to nuclear recoils making them visible in dark matter detectors, while many recoils from $\alpha$-induced neutrons fall below detector energy thresholds; (3) a detector can be protected against neutrons from the rock activity by hydrocarbon material, possibly with the addition of a thermal neutron absorber; such material, however, will also be a target for cosmic-ray muons.

This work includes, for the first time, a detailed Monte Carlo simulation of production, propagation and detection of neutrons from known sources, investigation of techniques for neutron flux suppression and studies of systematics associated with the neutron background in connection with the sensitivity of a future detector to WIMP-nucleus interactions. The work is part of a programme of neutron background studies for the dark matter experiments at Boulby mine (North Yorkshire, UK) (see Ref. [1] for a review of dark matter searches at Boulby). Similar studies have been initiated for dark matter experiments at Gran Sasso and Modane [2,3]. The present simulations were carried out for a large-scale xenon detector and are relevant to several programmes around the world, including other potential large-scale dark matter detectors. A tonne-scale xenon dark matter detector is planned for the Boulby Underground Laboratory [4]. A similar detector has been proposed for a new underground laboratory in the USA [5]. Another liquid xenon based detector is XMASS II [6] to be built in Japan for solar neutrino, double-beta decay and dark matter searches. The double-beta decay experiment EXO [7] will also be based on liquid xenon. The simulations presented here are important for many detectors designed for rare event studies.

The paper is organised as follows. Generation of neutron spectra from $(\alpha, n)$ reactions is described in Section 2. Neutrons from rock and the required shielding are discussed in Section 3. Simulations of muon-induced neutrons are presented in Section 4. Neutron background from detector elements is investigated in Section 5. Systematic effects caused by neutron background in connection with the sensitivity of a large-scale xenon detector to WIMP-nucleon cross-section are studied in Section 6. The summary and conclusions are given in Section 7.

## 2. Neutron production by radioactive isotopes

Neutron production by radioactive isotopes in the decay chains of uranium and thorium was

calculated using the SOURCES code [8]. The main features of the code are as follows. Spontaneous fission (of $^{238}$U mainly) was simulated using a Watt spectrum [9]. Neutron fluxes and spectra from $(\alpha, n)$ reactions were obtained taking into account the lifetimes of isotopes, energy spectra of alphas, cross-sections of reactions as functions of alpha energy, branching ratios for transitions to different excited states, stopping power of alphas in various media, and assuming isotropic emission of neutrons in the centre-of-mass system.

SOURCES provides a treatment of $(\alpha, n)$ reactions only up to 6.5 MeV $\alpha$-energies. This is likely to restrict significantly the reliability of the results because the cross-sections of $(\alpha, n)$ reactions rise with energy and the average neutron energy also increases with the parent alpha energy. Hence, the 6.5 MeV cut reduces the total neutron yield from $(\alpha, n)$ reactions and artificially shifts the neutron spectrum to lower energies. The effect of the neutron spectrum shift can be significant. We tested this by generating neutron spectra in NaCl with the original SOURCES code and by taking a different spectrum from Ref. [10], calculated for the Modane rock. We then propagated neutrons with both of these spectra through lead and various thicknesses of hydrocarbon material ($CH_2$) usually used to shield detectors from rock neutrons (see Section 3 for details of propagation procedure), and compared the two results. Even if both spectra are normalised to the same neutron production rate, there remains about a two order of magnitude difference in the predicted neutron flux above 10–100 keV after 30 cm of lead and 35 g/cm$^2$ of hydrocarbon, the spectrum from SOURCES giving a lower rate because of the smaller neutron energies. The effect is mainly due to the decrease in neutron–proton elastic scattering cross-section with energy. It became obvious that the neutron production code had to be modified to provide a more realistic treatment of $(\alpha, n)$ reactions. Note that the neutron production was simulated in Ref. [10] assuming a transition of the nucleus to the ground state only (this overestimates the neutron energy) and an emission of a neutron at 90° (which means that neutron energy was directly calculated from the alpha energy and the neutron spectrum was a delta-function).

The following modifications were made to SOURCES to overcome the 6.5 MeV limit. Existing cross-sections were extended to 10 MeV, taking into account available experimental data. For some materials, new cross-sections were added to the code. For example, we added the cross-section for $^{23}$Na measured up to 10 MeV [11] as an alternative to those already present in the code library. The cross-section for $^{35}$Cl was not present initially in the code library and was added from Ref. [12]. The cross-sections on Na and Cl were needed for calculation of neutron production in the salt rock. If the cross-section for a material was measured or calculated for low energies only, then it was extrapolated from low energies up to 10 MeV. The Nuclear Data Services of the Nuclear Data Centre at the International Atomic Energy Agency [13] were extensively used to obtain cross-sections.

The branching ratios for transitions to the ground and excited states above 6.5 MeV were chosen to be the same as at 6.5 MeV. This resulted in a small overestimate of neutron energies for alphas above 6.5 MeV, since the increased probability of transition to the higher states was neglected, but the total neutron flux was not affected. The uncertainties associated with the calculations of such probabilities were not negligible, however. The differences as large as (20–30)% exist between different calculations of the transition probabilities in the SOURCES library. If the excited levels were not in the code library, as was the case for elements for which the cross-sections were absent too, then in adding the cross-section we assumed that the transition was occurring to the ground state only.

## 3. Neutrons from rock

Here, our main objective was to find the thickness of hydrocarbon shielding needed to suppress the neutron flux from rock down to a level allowing the required sensitivity to WIMP-nucleus interactions. We started with neutron production in rock, then we propagated neutrons through the rock to the rock/cavern boundary and further on through lead and hydrocarbon shielding to the detector. Finally we generated nuclear

recoils from neutrons in the xenon target within the detector.

Simulation of neutron production via spontaneous fission and $(\alpha, n)$ reactions in rock was carried out with the modified SOURCES code (see Section 2). Rock was assumed to be halite (NaCl), which is the case for the Boulby Underground Laboratory (UK) and the Waste Isolation Pilot Plant at Carlsbad (USA), both being the proposed sites for underground experiments. The contamination levels of radioactive elements in rock vary from site to site and can vary also from hall to hall within an underground laboratory. In these simulations they were taken as 60 ppb of U and 300 ppb of Th in secular equilibrium. The energy spectrum of neutrons at production from SOURCES is shown in Fig. 1. The total neutron production rate was found to be about $1.05\times10^{-7}$ $cm^{-3}\,s^{-1}$. The neutron energy spectra in NaCl obtained with SOURCES are similar in shape for U and Th initiated neutrons (see Fig. 1). This means that for other contamination levels of U and Th the spectrum of neutrons (as well as the spectrum of nuclear recoils in a detector) can be scaled from that reported here taking into account the difference in contamination levels. For equal concentrations in NaCl, uranium gives roughly twice as many neutrons as thorium. For 100 ppb of uranium the neutron production rate is equal to $5.2\times10^{-8}$ $cm^{-3}\,s^{-1}$, whereas for a 100 ppb of thorium it is $2.5\times10^{-8}$ $cm^{-3}\,s^{-1}$. Decreasing the Th level down to 150 ppb (50% of the basic value used in the present work) results in a decrease of the neutron yield down to about 65% of the initial value with only a tiny decrease of the mean neutron energy from 1.81 MeV down to 1.75 MeV.

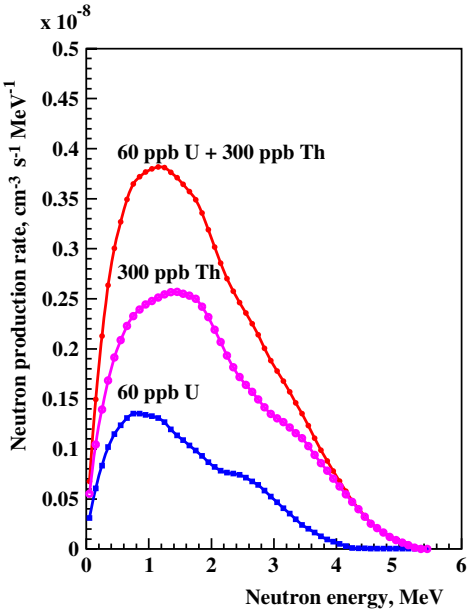


Fig. 1. Neutron energy spectrum from U and Th traces in rock as calculated with modified SOURCES. Contributions from 60 ppb U (filled squares and lower curve), 300 ppb Th (open circles and middle curve) and the sum of the two (filled circles and upper curve) are shown.

Neutron propagation through the rock was simulated using the GEANT4 package [14]. Neutrons from the rock wall were produced in a slab of rock $1\times1$ $m^2$ with 3 m depth into the rock (simulations with varying rock thicknesses showed that only those neutrons within 3 m of the rock surface are capable of reaching it). Neutrons from this region were allowed to propagate isotropically into a much larger region ($100\times100$ $m^2$ also with 3 m depth). This avoids neutron losses due to rock edge effects. The total spectrum observed from this region was then re-scaled to the original $1\times1$ $m^2$ surface element. Parameters of neutrons reaching the rock/cavern boundary were stored and neutrons were propagated later through lead and hydrocarbon shielding.

Neutrons were also simulated in a realistic cavern with a size of $30\times6.5\times4.5$ $m^3$ in the rock (see Fig. 2). The neutron flux at the rock/cavern boundary for this configuration was found to be $4.36\times10^{-6}$ $cm^{-2}\,s^{-1}$ above 100 keV and $2.20\times10^{-6}$ $cm^{-2}\,s^{-1}$ above 1 MeV. In practice these values are affected by the back-scattering of neutrons from other walls of the cavern: a neutron can enter the cavern, reach the opposite wall and be scattered back into the cavern increasing the total flux through the boundary. To check the effect of back-scattering, neutrons were propagated through the cavern and counted each time they entered the cavern. In this case the calculated neutron flux was $1.19\times10^{-5}$ $cm^{-2}\,s^{-1}$ above 100 keV and $4.10\times10^{-6}$ $cm^{-2}\,s^{-1}$ above 1 MeV. For a real detector the back-scattering of neutrons can occur also on detector elements, shielding etc.

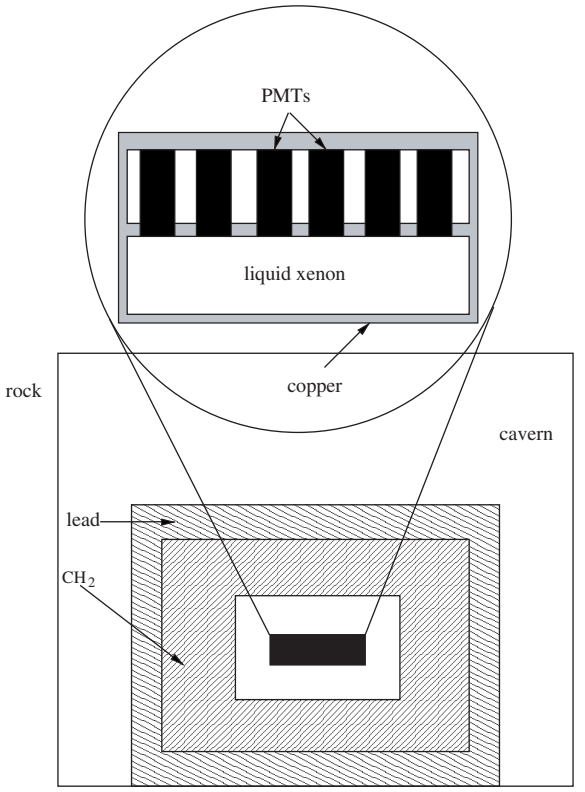


Fig. 2. Sketch of the laboratory hall with a xenon detector and shielding inside.

Lead of low radioactivity is widely used to shield dark matter detectors from gammas produced in the rock and the laboratory walls. Some detectors, however, can be made insensitive to these gammas [15]. So the use of lead as shielding and its thickness is decided for each particular experiment. Normally the thickness is such that gammas from rock contribute only a minor part to the total gamma flux at the detector, while a major contribution comes from the detector itself. Neutrons produced via spontaneous fission in low activity lead do not contribute significantly to the neutron flux coming from the rock. Simulations were carried out with and without lead shielding to investigate the effect of lead on the neutron flux. Neutrons coming from the rock in a simple geometry (neutron production volume—$1\times1\times3$ $m^3$, neutron propagation volume—$100\times100\times3$ $m^3$ as described above) were propagated through 30 cm of lead and those emerging on the opposite side were stored. Note that neutrons can be scattered back from the lead into the rock and then to the lead again. In order not to lose these neutrons the rock was present at this stage of the simulations, although the neutrons were generated only on its boundary. Then hydrocarbon shielding of varying thicknesses was added to the set-up after lead. Similar simulations were carried out without lead (with hydrocarbon only). Fig. 3 shows neutron spectra after 30 cm of lead and slabs of hydrocarbon of various thicknesses (Fig. 3a), and similar spectra obtained without lead (Fig. 3b). Due to the high cross-section of inelastic neutron scattering in lead above 4 MeV, the neutron spectrum after lead is suppressed at these energies. This results in a larger suppression of the neutron flux by the hydrocarbon when the lead is present compared to the case without lead.

The change in the neutron flux and spectrum can be expressed in terms of a suppression factor, which shows the ratio of the total neutron flux above a certain threshold after shielding to the initial flux. The suppression factors as functions of the thickness of hydrocarbon shielding for neutrons above 100 keV and 1 MeV are shown in Fig. 4. A lower neutron flux is expected if lead is used in the shielding together with the hydrocarbon material.

Present results agree with a preliminary simulation carried out with the MCNP code [16], in which lead, copper and hydrocarbon shielding were used [17].

From Fig. 4 we can conclude that using 35 g/$cm^2$ of hydrocarbon material together with 30 cm of lead or 50 g/$cm^2$ of hydrocarbon material without lead the neutron flux can be suppressed by about six orders of magnitude, which is a typical requirement to achieve a sensitivity to a WIMP-nucleon cross-section of about $10^{-10}$ pb. Lower (higher) fraction of hydrogen, compared to our basic $CH_2$ composition, requires larger (smaller) thickness of hydrocarbon material.

The precise thickness of hydrocarbon material to be used in the shielding depends on the geometry of a detector, target material, efficiency of neutron detection and the initial neutron flux (radioactive contamination of rock). Simulations

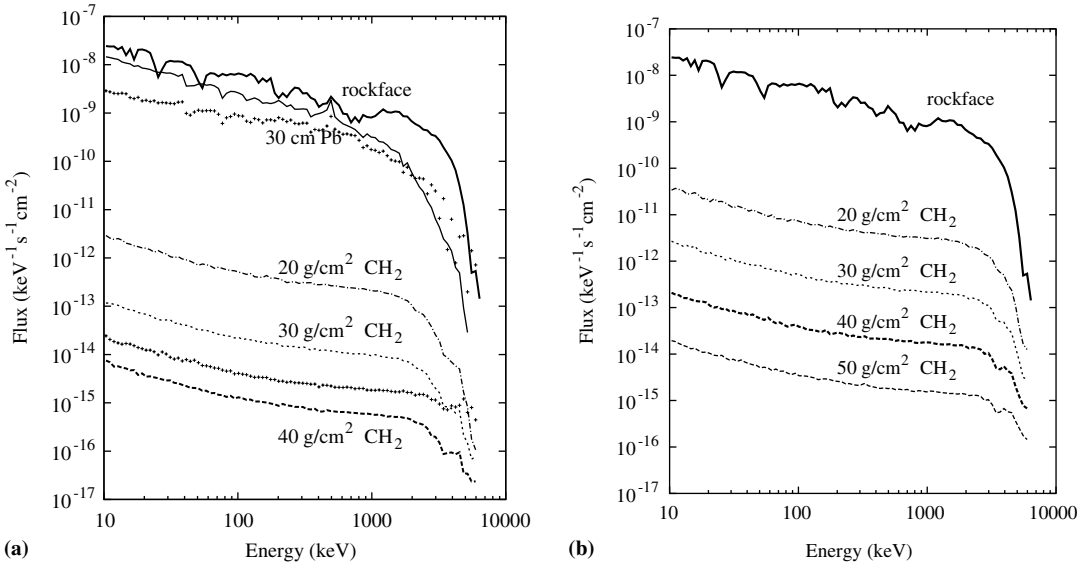


Fig. 3. Neutron energy spectra from rock activity after lead and hydrocarbon shielding: (a) with 30 cm of lead between salt and hydrocarbon; (b) without lead. Neutrons were propagated using GEANT4. The initial neutron production spectrum was obtained with modified SOURCES. Thick solid curve—spectrum at the salt/cavern boundary; thin solid curve—spectrum after 30 cm of lead (a); dash-dotted curve—spectrum after 20 g/cm$^2$ of hydrocarbon shielding behind lead (a) or without lead (b); dotted curve—spectrum after 30 g/cm$^2$ of hydrocarbon; thick dashed curve—spectrum after 40 g/cm$^2$ of hydrocarbon; thin dashed curve—spectrum after 50 g/cm$^2$ of hydrocarbon (b). Crosses show the spectra obtained with a neutron spectrum at the rock/cavern boundary from Modane measurements (see text for details): upper spectrum is for the flux after lead shielding; lower spectrum is for the flux after lead and 40 g/cm$^2$ of $CH_2$.

of the nuclear recoil energy spectrum in a large-scale xenon detector were carried out using the GEANT4 package with a neutron spectrum expected for the salt rock. The realistic geometry of the laboratory hall was taken into account (cavern size $30\times6.5\times4.5$ m$^3$). The neutron flux incident on the shielding around the detector is 2–3 times higher than in a simple geometry due to the back-scattering of neutrons from the walls. The energy spectrum of nuclear recoils expected in a 250 kg xenon detector (a cylinder with a diameter of 103 cm, height of 10 cm and density of 3 g/cm$^3$) surrounded by 35 g/cm$^2$ of hydrocarbon material and 30 cm of lead is shown in Fig. 5 by a solid line. The expected rate in a 10–50 keV recoil energy range (2–10 keV electron equivalent energy assuming a quenching factor of 0.2 for xenon recoils in xenon as reported in Ref. [18]) is 0.86 events per year. We conclude that 35–40 g/cm$^2$ of hydrocarbon and 30 cm of lead are enough to suppress the neutron flux from rock activity down to less than 1 event per year in a 250 kg xenon detector. As we will see below, this rate is sufficient to reach a sensitivity of about $10^{-10}$ pb to a WIMP-nucleon cross-section. If no lead is used, then 50 g/cm$^2$ is needed for a similar nuclear recoil rate in the detector and similar sensitivity.

If we assume the contamination levels to be 70 ppb U and 125 ppb Th (as recently measured in the new cavern at Boulby [19]), then the nuclear recoil rate in 250 kg of xenon behind 30 cm of lead and 35 g/cm$^2$ of hydrocarbon is about 0.56 events per year.

A shield made out of 30 cm of iron instead of lead suppresses the neutron flux by another order of magnitude after 35–40 g/cm$^2$ of hydrocarbon, but iron is less efficient for gamma absorption and typically has higher U/Th levels than lead.

To check the uncertainty of the results, we carried out similar simulations with the modified SOURCES code for Modane rock and compared them to the measurements of the neutron flux in

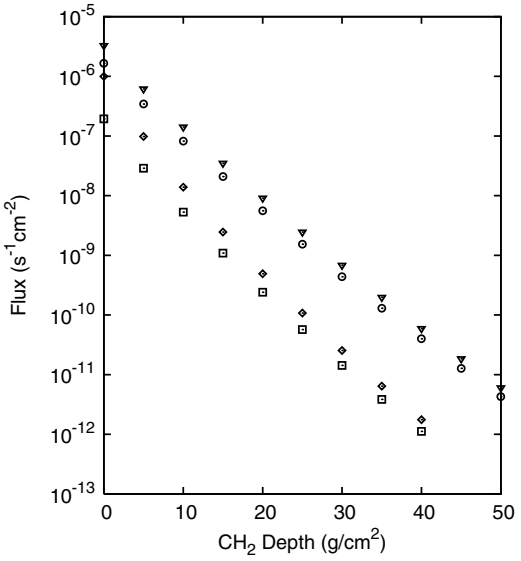


Fig. 4. Suppression factors for the total neutron flux above 100 keV and 1 MeV as a function of hydrocarbon thickness with and without lead shielding. Diamonds—flux above 100 keV beyond 30 cm of lead separating salt and hydrocarbon shielding; triangles—flux above 100 keV, no lead between salt and hydrocarbon shielding; squares—flux above 1 MeV, beyond 30 cm of lead between salt and hydrocarbon shielding; circles—flux above 1 MeV, no lead between salt and hydrocarbon shielding.

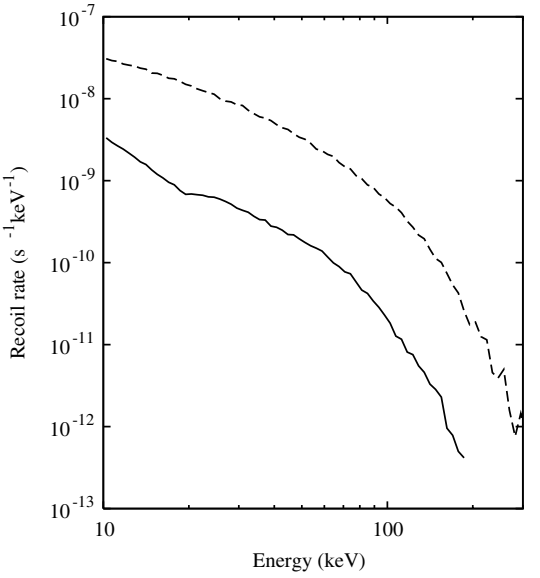


Fig. 5. Energy spectrum of nuclear recoils in a 250 kg liquid xenon detector from rock neutrons beyond 30 cm of lead and 35 g/cm$^2$ of hydrocarbon (see text for details). Dashed curve shows the recoil spectrum originated from input neutron spectrum from Modane measurements.

the Modane underground laboratory [10]. Using the contamination levels for rock from Ref. [10] we obtained a neutron production rate from $(\alpha, n)$ reactions of $8.11 \times 10^{-8}$ cm$^{-3}$ s$^{-1}$, which is about half the value calculated in Ref. [10], assuming the rock density of 2.7 g/cm$^3$. The difference is not great taking into account the uncertainties in the measured and evaluated cross-sections used, and the difference in the simulation strategy.

Fig. 6 shows the initial neutron production spectrum for Modane rock together with the spectra of neutrons at the rock/cavern boundary calculated with SOURCES (neutron production) and GEANT4 (neutron propagation), and measured at Modane [10]. The two spectra at the boundary look very different. The measured spectrum has a peak at about 3 MeV, similar to the neutron production spectrum in rock from SOURCES but shifted to higher energies. The spectrum of neutrons generated with SOURCES and propagated to the rock

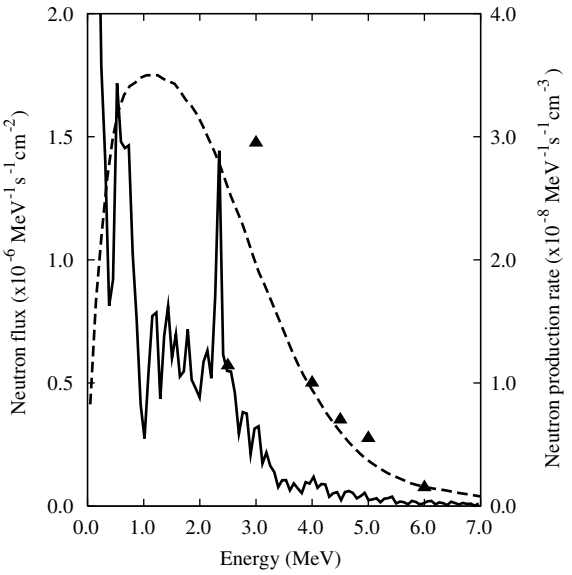


Fig. 6. Neutron production spectrum as calculated with modified SOURCES for Modane rock (dashed curve and right $y$-axis for rate units) is plotted together with the neutron energy spectra at the rock/cavern boundary: solid curve—spectrum from SOURCES propagated with GEANT4; triangles—evaluated spectrum from measurements [10].

surface with GEANT4 does not have a wide peak (the sharp peak at 2.3 MeV and various dips are due to the dip and peaks in the cross-section of neutron scattering on oxygen). The wide peak seen in the production spectrum has been smoothed by neutron interactions in rock. Note that the spectrum obtained in Ref. [10] is not a directly measured neutron spectrum. It was deconvolved from the measured proton recoil spectrum using a complicated procedure involving simulations including neutron propagation through the lead and copper shielding around the detector. Total neutron flux above 2 MeV has recently been re-evaluated, using more accurate simulations of the neutron propagation through the shielding and detector efficiency, and reduced from $4.0\times10^{-6}$ cm$^{-2}$ s$^{-1}$ above 2 MeV down to $1.6\times10^{-6}$ cm$^{-2}$ s$^{-1}$ [3]. The distortion of the neutron spectrum after Pb and Cu shielding (underestimated in Ref. [10]) was mentioned as the main cause of the difference in neutron flux [3] but no corrected spectrum was provided. A similar distortion in rock is responsible for a change of the neutron spectrum from that at production to that at the rock/cavern boundary as our simulations show (see Fig. 6). We believe that, although an obvious difference between our calculated spectrum and the measured one is observed, no definite conclusion can be derived about the correct shape of the neutron spectrum based on the existing data and simulations.

A wide peak (at about 2.2–2.3 MeV) in the measured neutron spectrum in the laboratory has also been reported recently in Ref. [20]. Here again the authors used the deconvolution of the measured spectrum of proton recoils and no simulation of the neutron propagation through the detector shielding was performed. No distinctive peaks have been reported for either of the measurements in the Gran Sasso Laboratory above 1 MeV [21,22], although the evaluated spectra appear to be harder than the spectrum from our simulations.

Having found a significant difference in the laboratory spectra (at the rock/cavern boundary) we studied the effect this may have on the neutron spectrum and nuclear recoil rate behind the shielding. We propagated neutrons with an energy spectrum from Ref. [10] for Modane rock through the shielding in a simplified geometry as described above (a slab of rock and slabs of shielding: 30 cm of Pb and 40 g/cm$^2$ of $CH_2$) and obtained neutron spectra behind the shielding shown by crosses in Fig. 3a (upper spectrum is behind 30 cm of Pb, lower spectrum is behind lead and 40 g/cm$^2$ of $CH_2$). The total neutron flux in the lab above 10 keV was taken as in our previous simulations to investigate the difference in the spectrum shape only. The nuclear recoil rate is proportional to neutron flux and the uncertainty in the total neutron flux can be easily propagated to the recoil flux. We assumed isotropic distribution of neutron directions at the rock surface within a hemisphere. After lead the 'Modane' spectrum is already not very much different in shape to the spectrum originated from SOURCES but is still harder. After lead and 40 g/cm$^2$ of $CH_2$ the 'Modane' spectrum below 1 MeV has similar shape to the spectrum originated from SOURCES but the neutron flux is three times higher. Above 1 MeV the difference in neutron flux is larger.

The effect is more dramatic if a realistic geometry of the cavern, shielding and detector is taken into account together with the production of nuclear recoils. We propagated neutrons from the rock through the cavern and shielding around the detector and calculated the spectrum of nuclear recoils in a detector. The cavern had a size of $30\times6.5\times4.5$ m$^3$, the detector was a cylinder with a diameter of 103 cm, height of 10 cm and density of 3 g/cm$^3$ surrounded by 35 g/cm$^2$ of hydrocarbon material and 30 cm of lead, as in our original simulations for recoil spectrum in xenon. The results are plotted in Fig. 5 (dashed curve). The spectrum is similar to the recoil spectrum originated from SOURCES, but the recoil rate in 10–50 keV energy range is 16 times higher (13.6 events/year). So, for a recoil flux in a realistic geometry, we obtained larger difference between our original spectrum and 'Modane' spectrum (Fig. 5) than for neutron flux in a simplified geometry (Fig. 3a). This large difference comes from the harder 'Modane' spectrum.

We conclude that, (i) realistic geometry of the cavern, shielding and detector is important for evaluation of the neutron suppression and nuclear recoil rate; (ii) a much harder neutron spectrum results in a significant increase in the recoil rate (in

our case the 'Modane'-type spectrum requires an additional 10–15 g/cm$^2$ of $CH_2$).

Special attention should be paid to the background associated with radon. Due to very high permeability of radon, it can penetrate through materials and contribute to the background in the target. Alpha background is briefly discussed in Section 6. Radon or its daughter's decay can occur in xenon close to the vessel wall or in the wall close to xenon with an alpha going out of the detector and a recoiling nucleus going into the detector and contributing to the low energy nuclear recoil rate. This effect is similar to that previously seen in some NaI(Tl) [23,24] detectors. These events can easily be rejected in a large xenon detector with position sensitivity.

Alphas from radon decay can also add to the neutron background in the vicinity of the detector, if radon penetrates through the shielding via the air gaps (large thickness of lead and hydrocarbon makes the diffusion of radon through the shielding unlikely). Materials surrounding the xenon target consist mainly of isotopes with a high threshold for $(\alpha, n)$ reactions, such as copper, iron, nitrogen and oxygen in air and carbon in hydrocarbon shielding. As a consequence of this, the neutron background from U/Th in these materials is dominated by spontaneous fission of $^{238}$U, with $(\alpha, n)$ reactions contributing about 20%. Radon and its daughters are free from spontaneous fission and only $(\alpha, n)$ reactions are the source of neutrons from radon decay. The main threat from radon is that if a significant fraction of rock produced radon is allowed to penetrate the shields, the alpha emitting progeny can be deposited close to the detector. Assuming a radon decay rate of about 1 Bq/m$^3$—a typical value for a ventilated laboratory, the neutron flux from alphas from radon decay can be a significant fraction of the flux from ultra-low-background PMTs discussed in Section 5. To suppress this flux, an appropriate protection against radon should be used, such as gas-tight sealing.

## 4. Muon-induced neutrons

Simulations of neutron production by muons with various energies in hydrocarbon material were recently performed by Wang et al. [25] using the FLUKA Monte Carlo code [26]. Kudryavtsev et al. [27] studied neutron production by muons in various materials with FLUKA using a calculated spectrum and an angular distribution of muons at the Boulby Underground Laboratory. This study is extended in the present work by including shielding materials and the production of nuclear recoils in the xenon detector.

The muon spectrum and angular distribution was simulated using the MUSUN Monte Carlo code (see Ref. [27] for description). Normalisation of the muon (and neutron) spectrum was done using the measured value for the muon flux at the Boulby Underground Laboratory: $(4.09 \pm 0.15) \times 10^{-8}$ cm$^{-2}$ s$^{-1}$, which corresponds to a rock overburden at vertical of $2805 \pm 45$ m w.e. [17,28]. The input surface muon spectrum was taken in the form suggested by Gaisser [29] with the parameters from the best fit to the LVD underground muon data [30]. For any other experimental site at similar depth, the neutron flux is scaled roughly as the muon flux. Variation of muon energy spectrum with depth can be accounted for by using the dependence of neutron production on the mean muon energy as $\propto E^{0.79}$ [27] (or $\propto E^{0.74}$ [25]). Changes in the neutron flux due to different rock composition around the laboratory (pure NaCl was used in this work) can be estimated following the dependence of the neutron production on the mean atomic weight of the rock as $\propto A^{0.76}$ [27].

Muons were sampled on the surface of a cube of rock (NaCl) $20 \times 20 \times 20$ m$^3$. The laboratory cavern of size $6 \times 6 \times 5$ m$^3$ was placed inside the salt region at a depth of 10 m from the top of the cube and at a distance of 7 m from each vertical surface of the cube. The cavern contained shielding made of lead and hydrocarbon material (see Fig. 2). Typical thickness was 30 cm of lead and 40 g/cm$^2$ of hydrocarbon material, corresponding to about 45–50 cm of liquid scintillator (active shielding) or about 40–45 cm of wax or polyethylene. The hydrocarbon was placed inside the lead so that it would absorb neutrons produced by muons in the lead. As will be shown below this is very important for shielding against muon-induced neutrons. A cylindrical vessel (103 cm diameter, 10 cm height) made of stainless steel of a thickness of 2 cm

containing 250 kg of liquid xenon (density 3 g/cm$^3$) was placed inside the shield. As iron and copper have similar atomic weights, substitution of iron with copper in a detector vessel will not change the neutron production in the vessel.

Simulations of muon propagation and interactions, development of muon-induced cascades, neutron production, propagation and detection were performed with FLUKA [26]. Tests of muon-induced neutron simulations with FLUKA can be found in [25,27]. The neutron production rate in NaCl at Boulby was found to be $7.6\times10^{-4}$ neutrons per muon per 1 g/cm$^2$ of muon path. The total neutron flux at the salt/cavern boundary is $8.7\times10^{-10}$ cm$^{-2}$ s$^{-1}$ above 1 MeV.

Fig. 7 shows the effects of lead and hydrocarbon material on neutron production and absorption. Neutron spectra on the rock/cavern boundary and after the lead (lead/cavern boundary) are presented in Fig. 7a. The large increase in the neutron spectrum after the lead, in particular below 1 MeV, is due to efficient neutron production in lead. Hydrocarbon material suppresses this flux by a large factor at low energies (Fig. 7b). This figure demonstrates the potential danger of placing the lead shielding close to the detector and inside the hydrocarbon shielding. Active veto systems may help to reject many events associated with muons but they cannot be 100% efficient if they are placed around the main detector and the lead shielding. The neutron flux is suppressed by a factor of $10^2$–$10^4$ by 40 g/cm$^2$ of hydrocarbon shielding at energies 0.1–10 MeV—most important for low-energy nuclear recoil production in xenon. To achieve similar suppression with active veto systems, they would need to have an efficiency up to 0.9999. This is very difficult to reach in practice, especially if the veto system is large and made of several modules. Another possibility is to use a single module veto detector placed just around the target. Such a detector, being made of hydrocarbon scintillator, can substitute for the passive absorber and provide additional rejection capabilities, which will be discussed later.

Neutrons produced in and around the detector can give nuclear recoils, which mimic WIMP-induced signals. Nuclear recoils produced via elastic scattering are of primary interest, since they are

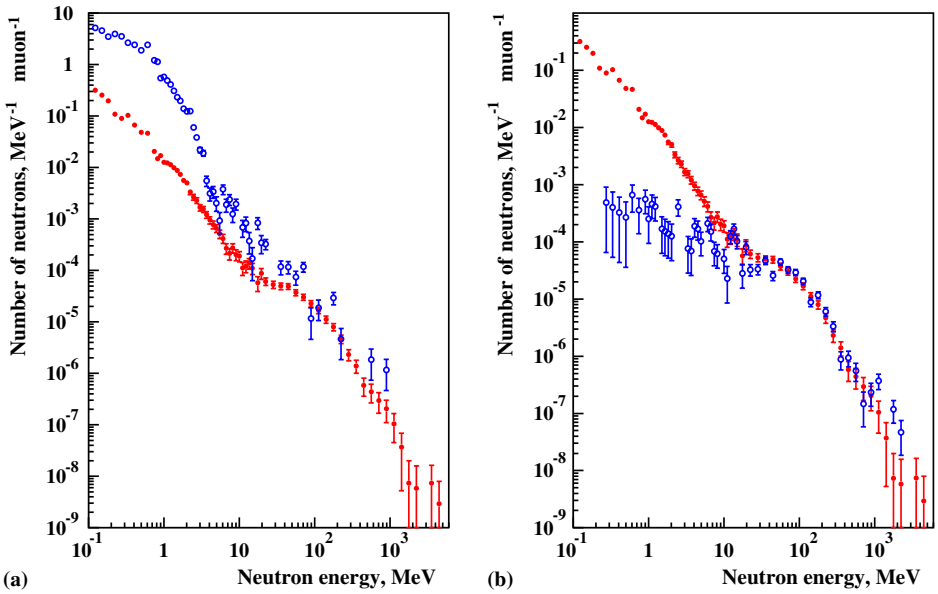


Fig. 7. Energy spectra of muon-induced neutrons at various boundaries: (a) filled circles—neutrons at the salt/cavern boundary, open circles—neutrons after the lead shielding; (b) filled circles—neutrons at the salt/cavern boundary (the same as in (a)), open circles—neutrons after the lead and hydrocarbon shielding.

not accompanied by gammas and cannot be discriminated from WIMP signals. Since many particles in addition to neutrons can give an energy deposition in a detector in any particular event (neutrons are produced mainly in muon-induced cascades), all of them should be followed to and through the detector with the same Monte Carlo code. Unfortunately, FLUKA does not generate nuclear recoils below 19.6 MeV neutron energy realistically. Kerma factors, equivalent to the average energy deposition, are calculated for neutron interactions. We modified this by assigning to the nuclear recoil an energy equal to the difference between initial and final neutron energies, which is correct for neutron elastic scattering. Since FLUKA uses a multigroup approach for low energy neutrons (below 19.6 MeV), the recoil energy is different from zero only if a neutron moves from one group to another one as a result of scattering. If this is not the case, then the nuclear recoil energy is taken from the initial FLUKA calculation of kerma factors. Such an approach is reasonable if there are several neutron interactions in the target and energies of recoils are summed, decreasing the uncertainty related to a single interaction. For single recoil events the statistical approach should be used with caution and the uncertainties associated with nuclear recoil treatment should be investigated in more detail.

Fig. 8 shows the energy spectrum of nuclear recoil events originated from muon-induced neutrons in a 250 kg liquid xenon detector. Events with multiple recoils were assigned an energy equal to the sum of the individual nuclear recoil energies, but excluding energy depositions due to processes not associated with neutron elastic scattering. The maximal distance between nuclear recoils in multiple recoil events is presented in Fig. 9. A significant fraction of the multiple recoil events have recoils separated by more than 10 cm. Rejection of multiple recoil events, which cannot be caused by WIMPs, should therefore be possible in liquid xenon detectors sensitive to the recoil position with sufficient accuracy.

About 20 million muons were simulated in total, which corresponds to a live time of 2.8 years. A total of 250 nuclear recoil events per year is expected in a 250 kg xenon detector. This also includes events where nuclear recoils are in coincidence with any other form of energy deposition in the detector not associated with nuclear recoils (electrons, photons, muons etc.). A rate of

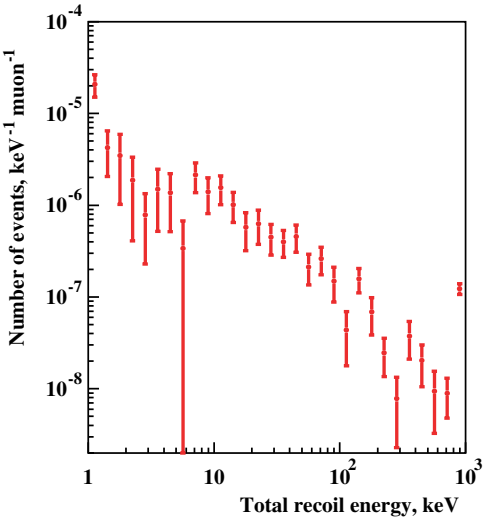


Fig. 8. Recoil energy spectrum in a 250 kg liquid xenon detector from muon-induced neutrons. The energy of all recoils in any particular event was summed to give the energy of each event. The highest energy point plotted also includes all events above 1 MeV.

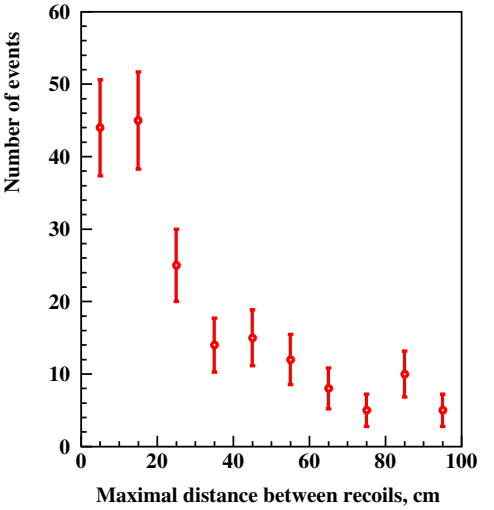


Fig. 9. Distribution of maximal distances between nuclear recoils in events occurring in a 250 kg liquid xenon detector from muon-induced neutrons.

25 events per year corresponds to nuclear recoils only without any other energy deposition. This is the number that determines the sensitivity of the detector to WIMPs, since other events will be rejected as electron-like events. Out of this, 11 events per year are single nuclear recoils. Finally, 7.5 nuclear recoil events per year (without electron-like component) are expected to be within an energy range of interest for dark matter searches (10–50 keV recoil energy or 2–10 keV measured energy with a quenching factor of 0.2 [18]). Less than a half of them are single recoils. This rate has an uncertainty associated with the treatment of nuclear recoil energy in FLUKA.

We also considered the possibility of using a scintillator made out of hydrocarbon material around the target as an active veto system (single module detector) against muon-induced events. To check the efficiency of such a veto only those events detected in anticoincidence between the main xenon detector and scintillator veto made of 40 g/cm$^2$ thick hydrocarbon were recorded. No events occurring in the target were detected in anticoincidence with signals in a hydrocarbon scintillator with an energy threshold of 100 keV.

Cosmic-ray muons and their secondaries will also add to the electron-like background in xenon. These events will be seen as high energy depositions and will be easily discriminated from expected nuclear recoil signal. Another problem is connected to the activation of some isotopes in detector components, including xenon isotopes, by cosmic rays (mainly neutrons) resulting in delayed (with respect to a muon) signals. This induced background, however, will contribute only a small part to the total gamma background from local radioactivity, which is expected to be rejected by discrimination.

Detector components, including xenon, can be activated at the surface by much higher cosmic-ray flux, prior to moving detector parts underground. Fortunately, xenon does not have long-lived radioactive isotopes and the background from xenon activation should not be a problem. Using powerful neutron sources underground for detector calibration may cause further activation of detector components. Activated isotopes will contribute to the expected electron-like background, which requires an accurate study in connection with a projected discrimination power of a future detector. The discussion of the discrimination power of a xenon dark matter detector is beyond the scope of this paper.

## 5. Neutrons from detector components

This is probably the dominant source of background, and is certainly the most difficult to calculate. It can come from the readout system, target, vessel walls, shielding, support structure etc.; for all these components the actual contamination levels are not known precisely. Figures for contamination levels supplied by manufacturers are usually approximate and can differ significantly from sample to sample. Measurements of contamination cannot be done for absolutely all components and again show quite large variations between samples. An example of this is the U/Th traces in PMT components. Here we used typical contamination figures provided by manufacturers together with measurements carried out by various experimental groups (see the UKDMC web-site [19] for references).

We considered here in detail photomultiplier tubes as probably the most important source of background for a liquid xenon detector. We assumed a detector made out of copper, for which U/Th levels are well below 1 ppb and do not pose a serious threat in terms of neutron background (also because of the high threshold of $(\alpha, n)$ reactions in copper). We will discuss this in more detail later on in this section. Concentrations of U and Th in the hydrocarbon material of the shielding may be slightly higher, but $(\alpha, n)$ reactions can occur only on $^{13}C$ (due to the high threshold of reaction on $^{12}C$), which is only 1.1% of the carbon isotopic composition. Moreover, hydrocarbon is very efficient at slowing down sub-MeV neutrons and most of it is further away from the xenon target than many other components. If used as an active veto system, hydrocarbon could provide a coincidence signal: proton recoil from neutron scattering and/or thermal neutron capture by a proton or by an additive element with a large neutron capture cross-section, for example Gd.

Table 1
Materials used in PMTs with their weights, contamination levels of U and Th, neutron production rates from U and Th impurities in PMTs, and nuclear recoil rates per (kg×year) of target exposure (10-50 keV recoil energy) from various components for ETL 9266 and Hamamatsu R8778

| Material | Mass, g | U, ppb | Th, ppb | Neutrons (U), $cm^{-3}\ s^{-1}$ | Neutrons (Th), $cm^{-3}\ s^{-1}$ | Rate (U), $kg^{-1}\ year^{-1}$ | Rate (Th), $kg^{-1}\ year^{-1}$ |
|---|---|---|---|---|---|---|---|
| ETL 9266 | | | | | | | |
| Borosilicate | 70 | 30 | 30 | $7.5\times10^{-9}$ | $2.3\times10^{-9}$ | 0.78 | 0.25 |
| Ceramics | 10 | 50 | 60 | $1.45\times10^{-8}$ | $7.8\times10^{-9}$ | 0.1 | 0.08 |
| Metals | 20 | 0 | 30 | 0 | $4.5\times10^{-10}$ | 0 | 0.004 |
| R8778 | | | | | | | |
| Quartz | 7 | 4 | 4 | $2.2\times10^{-10}$ | $4.8\times10^{-11}$ | 0.002 | 0.0004 |
| Metals | 153 | 4 | 4 | $4.8\times10^{-10}$ | $6.0\times\ 10^{-11}$ | 0.024 | 0.004 |

Xenon itself can be purified to reduce the neutron background from spontaneous fission to a very low level. Remaining neutron-induced events can be discriminated using energy deposition of fission products, which will occur at a location separated from neutron-induced recoil. These considerations show that with the standard PMT readout, the PMTs and their bases (including high voltage dividers) should constitute the most serious limitations to the detector sensitivity.

Two types of PMTs were used to simulate PMT related neutron background. The 2-in. ETL type 9266 PMT (the actual diameter of the PMT is 5.2 cm) with low contamination levels of U and Th [31] (see Table 1 for details) was modelled as a cylinder made out of glass, metals and ceramics. Similarly, the newly designed 2-in. Hamamatsu R8778 tube [32] (the actual diameter of the PMT is 5.7 cm) was modelled as a cylinder made out of quartz glass and metals. A cylindrical xenon detector, similar to those described in Section 3 (see Fig. 2), was viewed by either 217 ETL 9266 PMTs or 169 R8778 PMTs. The total area of the detector covered by the PMTs is similar in both cases. The hydrocarbon material is placed between PMTs to reduce neutron flux. Note that the window in the standard version of the ETL 9266 PMT is made out of borosilicate glass and cannot be used for detection of VUV light from xenon. The solution to this problem, which does not lead to an increase in contamination due to the use of impure materials, is to coat the window with a wavelength shifter. The contamination levels for the ETL 9266 PMT were taken from [31]. Radioactive impurities in the R8778 PMTs were estimated based on measurements of activity concentrations from Ref. [32]. Different measurements, however, lead to different contamination levels ranging from about 2 to 10 ppb of U and Th for the metal PMT of weight 160 g. We assumed the contamination levels to be 4 ppb U and 4 ppb Th. We estimated the proportion of glass and metals in R8778 from similar figures for other PMTs of similar size. Note that the weight of metal in the R8778 as well as its total weight is larger than that for the ETL 9266 because the whole envelope of the R8778 is made out of metal (we assumed everywhere that the metal of the PMT is stainless steel).

The modified SOURCES code (see Section 2 for details) was used to obtain neutron spectra from the various materials. The material component of each PMT was populated separately with the neutron spectrum from SOURCES and this spectrum was then emitted isotropically and propagated through the detector. The set-up included 1 cm thick copper walls around the liquid xenon and PMTs, a 1 cm thick copper support structure for the PMTs and an acrylic (plexiglass or PMMA) absorber between PMTs to suppress the neutron flux (see Fig. 2). If a neutron scattered two or more times in xenon target, the energies of all recoils were added up to obtain the total measured energy of the event. In the calculation of recoil rates and sensitivities we assumed again that a detector had a step function energy threshold of 2 keV (10 keV recoil energy with a quenching factor of 0.2) and we used a 2–10 keV measured energy range. The statistics for all simulations described in this

Section correspond to a live time of more than 1000 years of running.

Table 1 summarizes the contamination levels from PMT components [31,32] and the simulation results. Statistical errors for all figures in the table do not exceed 5%. The total error is dominated by systematics related to uncertainty in the contamination levels of detector components. Such an uncertainty can be as high as a factor of 2. About 300 events per year at 10–50 keV recoil energies are expected in a 250 kg xenon detector from 217 ETL 9266 PMTs covering about a half of the xenon surface. (Note that this number is more than an order of magnitude higher if standard, not low background, PMTs are used, which is not acceptable for a sensitive detector.) Only 7.6 neutrons per year can be detected with 169 R8778 tubes. Fig. 10 shows the energy spectrum of nuclear recoils produced by neutrons from the R8778 PMTs.

Several methods can be used to reduce these numbers. Five centimeter thick acrylic (plexiglass) lightguides between PMTs and xenon can reduce the nuclear recoil rate from PMTs by a factor of 2, giving 3.6 events per year from all R8778 PMTs. Acrylic is known to have a very low level of impurities. Contaminations of U and Th at a level of $10^{-12}$ ppb have been achieved by the SNO Collaboration [33], so the neutron flux from the lightguides can be negligibly small. However, the use of the lightguides reduces the light collection.

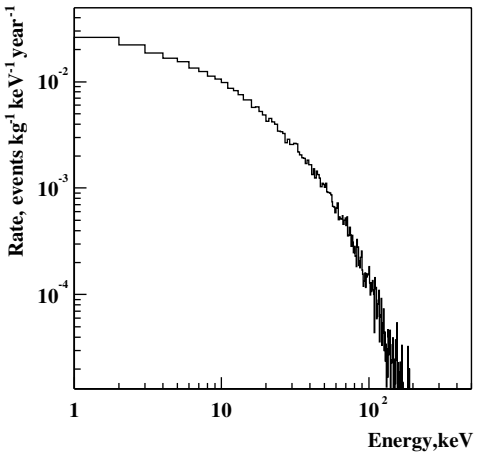


Fig. 10. Energy spectrum of nuclear recoils produced by neutrons from R8778 PMTs in a 250 kg liquid xenon detector.

Moreover, acrylic is not transparent to VUV radiation and therefore a waveshifter coating for lightguides is needed.

Reducing the contamination levels of PMTs and making these PMTs of larger (5-in.) size will improve the sensitivity of future detectors. Contamination levels of 1 ppb for both U and Th can reduce the neutron background rate in the detector from PMTs to 0.9 events per year. The use of PMTs with a larger diameter photocathode (5-in.) and similar impurity levels can further reduce the nuclear recoil rate bringing it down to about 0.4 events per year, by reducing the total weight of PMT material.

Let us now consider other sources of neutrons in the detector. High voltage dividers required by PMTs, with standard resistors and capacitors, can have high background radioactivity. Although the mass of ceramics used in them is small, the level of impurities reaches 100–1000 ppb of U and Th, giving a rate potentially comparable to that expected from the PMTs themselves. A way around this is to use chip resistors and film capacitors with lower levels of radioactive impurity and to move them further from the target [32], bringing the number of events from this source below the PMT contribution. Note that use of the hydrocarbon between PMTs and as lightguides will also reduce the number of events from dividers.

Although the copper vessel is assumed to be heavy (1 cm thick walls were used in the simulations giving the total weight of copper of 350 kg), it should not give a major contribution to the neutron background. The radioactive impurities in some copper samples were found to be below 0.02 ppb [19]. With such a level of impurity (0.02 ppb) the nuclear recoil rate is about 0.4 events per year, which can be slightly reduced by PTFE (teflon) reflectors, which may be required between the copper vessel and xenon target. PTFE itself contains less than 1 ppb of U and Th and its weight can be reduced to bring the neutron rate to below 1 event per year.

Further, more precise measurements of the radioactive impurities in various material samples used in the detector construction are needed.

Adding up contributions from the main detector components we can conclude that the total rate

of neutron-induced nuclear recoils, achievable at the present level of technology, is of the order of 4–8 events per year in 250 kg of liquid xenon (10–50 keV recoil energy).With provisional success in PMT developments and the use of other ultra-pure materials (for instance, ultra-pure copper) the rate can be reduced to about 1 event per year (see Table 2).

Similar or even larger reduction in the background could be achieved with new readout designs, such as GEM [34] or MICROMEGAS [35], without PMTs and associated background, currently being studied for large dark matter detectors [36,37]. Materials, such as copper, kapton and teflon, all with very low levels of impurities can be used reducing the number of expected events to less than 1 event per year (see Table 2, Detector 5 described in Section 6).

Another possibility to suppress the background is to estimate it by independent techniques and subtract the estimated value from the measurements. In practice, this can be done using statistical tables [38] for the upper limits on a signal at a certain confidence level as functions of the measured number of events and estimated background (neutron-induced nuclear recoils). The following methods to estimate the background can be used.

Due to the very small interaction cross-section, a WIMP should produce no more than one nuclear recoil per event. A neutron can produce one or more recoils, but only events with a single recoil can mimic WIMP interactions if a detector has position sensitivity. Fig. 11 shows the expected multiplicity distribution of recoils (with an energy threshold of 10 keV for each recoil) for low background PMTs and Fig. 12 shows the number of events with multiple recoils as a function of maximal distance between recoils. Note that multiple recoils here are produced by the same neutron, whereas similar events from muon-induced neutrons can be due to several neutrons generated in the same cascade. The rejection of multiple recoil events not only reduces the background by more than 60% (37% of the initial value—exact number depends on the position sensitivity of a detector) but also provides a method of calculating the expected single recoil rate from neutrons. Single and multiple recoil rates depend on the same factors, such as neutron interaction cross-section, detector geometry and detector response. Matching the calculated multiple recoil rate due to neutron interactions with measurements, we can then estimate the expected single recoil rate due to neutrons and subtract it from the measured single

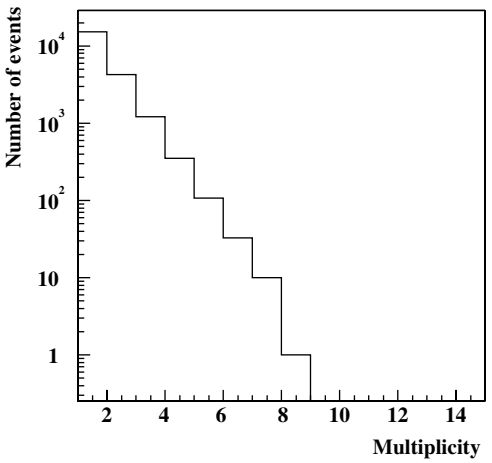


Fig. 11. Distribution of nuclear recoil multiplicities in events caused by R8778 PMT neutron background in a 250 kg liquid xenon detector. The first bin corresponds to single recoil events. In this particular case an energy threshold of 10 keV for each nuclear recoil in an event (not for the sum of the recoil energies in an event) was applied.

Table 2
Neutron background rates per year in a 250 kg liquid xenon detector for five different configurations (see text for details)

| Configuration | 1 | 2 | 3 | 4 | 5 |
|---|---|---|---|---|---|
| Rock neutrons | <0.2 | <0.2 | <0.2 | <0.2 | <0.2 |
| Neutrons from muons | 7.5 | 3.3 | <0.8 | <0.8 | <0.8 |
| PMTs | 7.6 | 2.8 | 2.8 | 3.6 | 0.4 |
| Copper vessel | 0.4 | 0.2 | 0.2 | 0.4 | 0.4 |
| Total | 15.5 | 6.3 | 3.0 | 4.0 | 1.0 |

Contributions from the main sources of neutron background are shown separately together with the total rate.

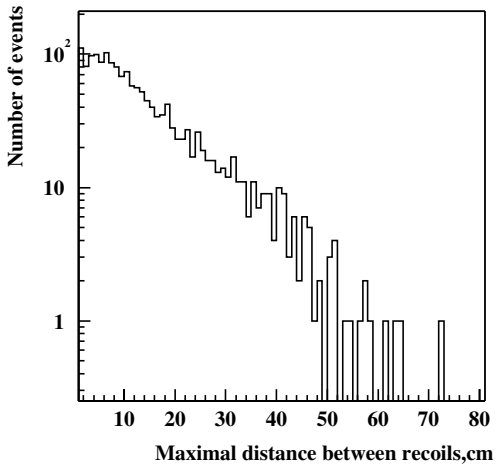


Fig. 12. Distribution of maximal distances between nuclear recoils in events occurring in a 250 kg liquid xenon detector due to neutrons from R8778 PMTs.

recoil rate. Note that a similar technique was applied to subtract neutron-induced background in the CDMS experiment [39].

Some improvements in the estimate of the neutron background may come from measurements of the energy spectrum of recoils. This, however, needs further study, in particular detailed comparison of simulated spectra from neutrons and from WIMPs with various masses. Also it is not obvious that appropriate statistics in real data will be available to make this method work.

Finally, if the hydrocarbon material around a xenon detector is in fact an active veto system, then some neutrons will give signals in both the target and veto detectors, as discussed in Ref. [40]. Rejecting those events produced by neutrons, we can also use their rate and spectrum as a basis for calculating the single recoil rate in xenon and again subtract an estimated neutron signal from the measured recoil rate.

All these methods combined together should provide an unambiguous estimate of the neutron-induced nuclear recoil rate and grounds for statistical neutron background subtraction. In the case of complete matching between the measured and predicted background rates, the errors of each added in quadrature result in a total error, which is proportional to the square root of the measured rate. For example, having 300 events during one year of experiment live time (as in the case of ETL 9266 PMTs) and expecting a similar number from neutrons, we can calculate the mean value of WIMP-induced events (with full background subtraction) as around 0 with the standard deviation of $\sqrt{2 \times 300} = 24.5$ and a limit at 90% confidence level (CL) of about 40. Hence, a factor of 8 reduction is expected with a full statistical subtraction of the neutron-induced background. For a measured number of 4 events during 1 year of detector running time the statistical tables [38] can be used to obtain an upper limit on a signal rate, which is 4.6 if the estimated background is exactly equal to the measured rate.

## 6. Bounds on WIMP sensitivity of large-scale xenon detectors from neutron background

Events induced by neutrons in the detector, which mimic WIMP-produced nuclear recoils, can be considered as a crucial factor that limits detector sensitivity. Based on the above results it is worth estimating the limits on WIMP-nucleon cross-section, which can be achieved with various rates of neutron-induced events, as a means to aiding the design of future detectors and improving their characteristics.

Gamma background may also be a limiting factor. Gamma background is higher by several orders of magnitude (mainly due to internal contamination of the target and, possibly, PMTs) than neutron background after shielding, but techniques are being developed, which give efficient discrimination between electron and nuclear recoils. The rate of gamma events remaining after rejection depends on the discrimination power, which is a characteristic of a particular detector. Typically a factor of $10^7$ suppression is required to achieve sensitivity down to $10^{-10}$ pb at the minimum of the sensitivity curve. However, the statistical suppression factor, defined as the ratio of the gamma background rate to the limit on the nuclear recoil rate, can be much higher than the discrimination power deduced on an event-by-event basis, often called the figure of merit. Use of $^{85}$Kr free xenon and other pure materials can soften this requirement by 2–3 orders of magnitude. ZEPLIN

I, a liquid xenon detector at Boulby, already achieved the statistical suppression factor of about $10^3$ [41]. Consideration of the gamma background and discrimination power is, however, beyond the scope of this work. We assume instead that gamma background is discriminated against nuclear recoils so that it does not produce serious problems for detector sensitivity.

Alphas can also contribute to background events at low energies. Although they typically deposit a few MeV in the target, converted into an MeV signal after correction for quenching, some of them can be emitted close to the surface of the target and so lose energy in a keV range. For those originating within the xenon, it is possible for only a small fraction of their energy to be deposited inside the target (accompanied by a nuclear recoil energy deposition), the remaining energy being lost in the vessel walls, where it is not detected. In a similar way, alphas emitted in the vessel or PMTs close to the surface can deposit a large fraction of their energy there, enter the target and deposit a remaining small fraction in the xenon, which will be detected. In both cases the events can be misinterpreted as low energy nuclear recoil events, unless a topological study reveals that the events occured close to the surface of the target and/or the discrimination between nuclear recoils and alphas allows complete rejection of alpha events. We will assume here that xenon purification, discrimination between nuclear recoils and alphas, and topology study will reduce alpha background down to a non-observable level.

Neutrons from radioactivity in rock and laboratory walls can be absorbed down to a level of less than 0.2 events per year by about 40 g/cm$^2$ thick slab of hydrocarbon placed behind lead shielding (between lead and detector). In the case of the harder neutron spectrum, larger thickness of $CH_2$ may be needed. This is the main result of Section 3. So, the rate of events due to this source of background will be negligibly small. Radon can be kept away from the detector by using gas-tight sealing.

For muon-induced neutrons it is worth considering two cases: (i) passive hydrocarbon shielding around the detector, and (ii) an active veto system with liquid or plastic scintillator between lead and the detector (which can act as gamma, neutron or muon veto). For case (i) 7.5 events per year with measured energies between 2 and 10 keV are expected in a 250 kg xenon detector. Note that some uncertainty remains because of the simplified treatment of the nuclear recoil energy in FLUKA. The rate can be as small as half that value if the event topology study rejects most multiple recoil events. This sample is a small fraction of events associated with cosmic-ray muons. Providing the agreement between measurements and simulations is reached for all these events, as well as for multiple recoil events without electron recoils, a statistical subtraction of this background can be done, improving the detector sensitivity. For case (ii) less than 0.8 events per year (at 90% CL) are expected independently of the recoil spectrum (the accuracy is restricted by the statistics of the simulations).

The neutron background from detector components depends largely on the readout components. With standard UV PMTs (with quartz window and graded seal giving a high background—not considered in detail here) the rate of background events (several thousand events per year at 2–10 keV measured energy in a 250 kg detector) is too high and allows only a sensitivity of $10^{-7}$ pb to be reached at the minimum of the sensitivity curve. Although statistical background subtraction can reduce this limit by more than an order of magnitude, it is obvious that these PMTs cannot be used in future large-scale dark matter detectors.

Low background ETL 9266 PMTs will produce about 300 events per year at 2–10 keV measured energy in a 250 kg xenon detector. A factor of 8 reduction in limit can be achieved if the measured spectrum and multiplicity of these events agree with simulations, providing a good reason for statistical subtraction of this background. A liquid scintillator veto around the detector (instead of or in addition to the passive shielding) can be used in anticoincidence with the main xenon detector allowing rejection of events with nuclear recoils in both target and veto system. Again, accurate simulations of the coincident events will help to estimate the remaining background and statistically subtract it from the measured rate.

Ultra-low-background Hamamatsu R8778 PMTs would yield background rates of 4–8 events per year depending on whether neutron absorbing lightguides are used. Active veto system around the target should reject some fraction of events induced by neutrons from detector components. The simulation of veto efficiency for these events is the subject of a separate study.

Further improvements in PMTs discussed in the previous section can reduce the background rate to probably less than 1 event per year. New readout techniques, such as GEM [34] or MICROMEGAS [35], are of potential interest because they may help to avoid using PMTs with their relatively high level of radioactivity. Without PMTs the remaining neutron background comes mainly from the copper vessel and gives a total rate of less than 1 event per year.

Table 2 shows the summary of the neutron background rates in a 250 kg xenon detector for five different detector configurations as follows:

*Configuration 1*: 169 R8778 PMTs (4 ppb of U and Th), no lightguides, passive shielding around the detector (30 cm of lead and 40 g/cm$^2$ of hydrocarbon), single and multiple recoils induced by neutrons.

*Configuration 2*: 169 R8778 PMTs (4 ppb of U and Th), no lightguides, passive shielding around the detector (30 cm of lead and 40 g/cm$^2$ of hydrocarbon), only single recoils induced by neutrons are counted.

*Configuration 3*: 169 R8778 PMTs, no lightguides, passive and active (to reject muon-induced neutrons) shielding around the detector (30 cm of lead and 40 g/cm$^2$ of hydrocarbon), only single recoils are counted.

*Configuration 4*: 169 R8778 PMTs, acrylic lightguides, passive and active shielding around the detector (30 cm of lead and 40 g/cm$^2$ of hydrocarbon), both single and multiple recoils are counted.

*Configuration 5*: large PMTs with 1 ppb of U and Th, acrylic lightguides, passive and active shielding around the detector (we assumed 1 detected event instead of an average figure of 0.8 events per year if neutron contribution from rock and muons can be neglected). Similar numbers are expected from new readout techniques without PMTs, such as GEM or MICROMEGAS.

The rates at 2–10 keV electron equivalent energy range (10–50 keV nuclear recoil energy) are shown in Table 2. Rock neutrons are absorbed to a level of less than 0.2 events/year by passive and active shielding for all five configurations and are neglected for all detector configurations, as well as muon-induced neutrons for the configurations with an active veto system. A copper vessel with a weight of 350 kg is presumed to have 0.02 ppb of U and Th. Hydrocarbon material was placed between PMTs in all configurations. If a background rate can be estimated, as discussed in Section 5, then it can be statistically subtracted, reducing upper limits on nuclear recoils.

Fig. 13 summarizes the limitations on the sensitivity of a future 250 kg xenon detector running for a year for dark matter searches assuming 100% rejection of gamma and $\alpha$-induced events. Although future tonne-scale detectors are aimed at discovering WIMPs, we present the results in more conventional terms of limits on WIMP cross-section as a function of WIMP mass to allow direct comparison between different existing and planned detectors. An isothermal spherical halo with 0.3 GeV/cm$^3$ WIMP density and Maxwellian WIMP velocity distribution was assumed and the procedure described by Lewin and Smith [42] was followed. For any specific detector configuration (see below) the parameter space below the curve cannot be probed because of the neutron background. The dotted line shows the limitations on the sensitivity for a detector with 169 2-in. low background R8778 PMTs surrounded by a hydrocarbon passive shielding (about 15.5 background events per year at 2–10 keV measured electron equivalent

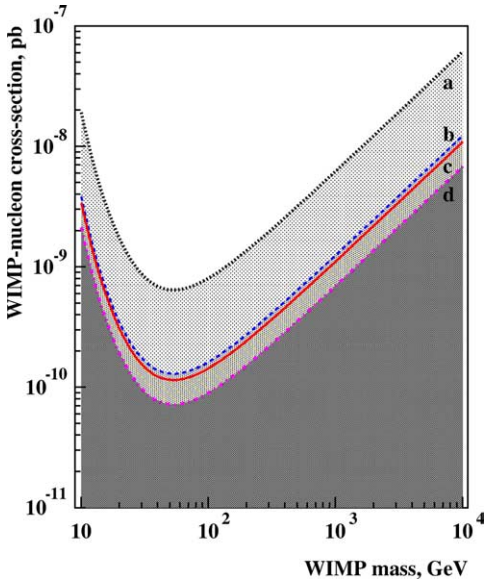


Fig. 13. Limitations on the sensitivity of a future 250 kg xenon detector (1 year running time) for dark matter searches assuming 100% rejection of gamma and α-induced events. For any specific detector configuration (see text for details) the parameter space below the curve cannot be probed because of the neutron background. Dotted curve (a)—detector with 169 2-in. ultra-low-background R8778 PMTs surrounded by hydrocarbon passive shielding (Configuration 1). Dashed curve (b)—detector with liquid scintillator veto system (Configuration 3); background is statistically subtracted. Solid curve (c)—detector with an active veto assuming further improvements in a PMT design (large PMTs with lower contamination levels, Configuration 5). Dashed–dotted curve (d)—ultimate limit for a detector with no background events observed during one year of running reachable with charge readout and ultra-pure materials.

energy from PMTs and muon-induced neutrons giving an upper limit of 21.9 events per year, as for Configuration 1). The dashed line corresponds to a detector with a scintillator veto system and all the background statistically subtracted (3.0 events per year for both measured and estimated background which corresponds to an upper limit at 90% CL of about 4.4 events per year, as for Configuration 3). The solid line shows the limit achievable by a detector with an active veto, lightguides and future new large PMTs with U/Th levels down to 1 ppb (about 1 event per year giving less than 3.9 events per year at a 90% CL, as for Configuration 5). A new type of readout technique (GEMs or MICROMEGAS) with very low levels of radioactivity (less than 1 event per year coming from the copper vessel) would provide a similar sensitivity. Finally the dashed–dotted curve shows the ultimate limit for a detector with no background events observed during one year of running, reachable with a charge readout technique and ultra-pure components, for instance, less than 0.01 ppb of U/Th in the copper vessel. The above figures can be scaled up to a larger detector. Assuming 0.01 ppb of U and Th in a 350 kg copper vessel is the only source of neutron background and a 250 kg liquid xenon detector has an infinite running time, the nuclear recoil rate in the detector is expected to be 0.2 events per year and the sensitivity to WIMP-nucleon cross-section, which can be achieved with such a rate without background subtraction, is about $6\times10^{-12}$ pb at the minimum of the sensitivity curve.

A step function energy threshold of 2 keV was assumed in the calculations of the sensitivities. This is, however, a specific parameter for any particular experiment. Lowering the energy threshold down to 1 keV may improve the sensitivity by about 50% if no background events below 2 keV are detected. In reality the trigger efficiency is not a step function and should be both measured and calculated for a particular detector. The energy resolution was taken as $1.24\sqrt{E}$ as measured for the ZEPLIN I experiment [43]. Note, however, that for xenon experiments the sensitivity at the minimum of the curve does not depend strongly on the energy resolution.

## 7. Summary and conclusions

Various sources of neutron background for a future large-scale xenon dark matter detector have been investigated. Shielding with 35–50 g/cm$^2$ of hydrocarbon (depending on the thickness of lead shielding and the neutron spectrum) is needed to suppress the neutron background from rock down to a level acceptable for a high sensitivity dark matter detector (less than 1 event per year in a 250 kg xenon detector).

Hydrocarbon is also very effective in suppressing the neutron flux induced by cosmic-ray muons in rock and lead (if lead shielding is placed

between the rock and hydrocarbon). Most events from muon-produced neutrons in the detector will contain not only nuclear recoils but also muons, photons and electrons associated with muon-induced cascades. Remaining neutron events can be rejected by anticoincidence with an active veto system placed around the detector (the hydrocarbon can be the liquid scintillator of an active veto system). Additional rejection of neutron-induced nuclear recoil events is possible through studying event topology, most neutron-induced events being multiple recoil events.

Standard photomultiplier tubes with quartz window and graded seal produce a high flux of neutrons from $(\alpha, n)$ reactions and hence cannot be used in detectors aimed to reach a sensitivity below $10^{-8}$ pb. Ultra-low-background tubes can generate about 4–8 nuclear recoil events per year in a 250 kg xenon detector. Other detector components can contribute a small fraction to the total background. Further improvements in PMTs (larger size and lower contamination levels) can bring this number down to less than 1 event per year.

Restrictions on the detector sensitivity associated with the neutron background have been studied. Neutrons from $(\alpha, n)$ reactions in rock and cosmic-ray muons do not limit the sensitivity to WIMP-nucleon interactions down to about $10^{-10}$ pb, especially if an active hydrocarbon veto (rather than passive shielding) is installed around the detector. Some detector components, such as PMTs (even ultra-low-background PMTs) and associated equipment, produce a noticeable flux of neutrons. This flux, however, does not limit detector sensitivity down to about $(1.3–1.5)\times10^{-10}$ pb at the minimum of the sensitivity curve if neutron absorbing lightguides are used, multiple recoils are rejected and statistical subtraction of background is possible based on comparison between measurements and simulations of spectra, multiplicity and topology of background events. Some events can be individually rejected by anti-coincidence with an active veto system. This needs further study.

The best way to improve the sensitivity is to use larger diameter PMTs with lower contamination level or an alternative technique for charge read-out based on materials with an ultra-low level of radioactivity.

## Acknowledgements

The work has been undertaken within the framework of the UK Dark Matter Collaboration (University of Edinburgh, Imperial College, London, Rutherford Appleton Laboratory and University of Sheffield) and contributes to the collaboration-wide simulation efforts. This work is funded by PPARC. The authors are grateful to Prof. P.F. Smith, Dr. N.J.T. Smith, Prof. T.J. Sumner, Prof. J.J. Quenby, Dr. J.D. Lewin, Dr. R. Lüscher, Dr. A.S. Howard, Dr. J.V. Dawson, Dr. H. Araujo, Dr. I. Liubarsky, Dr. A.St.J. Murphy, Prof. D.P. Snowden-Ifft and Prof. C.J. Martoff for valuable discussions. Special thanks are addressed to Prof. P.F. Smith, who performed comparison of our results with his simulations. The authors acknowledge useful comments from an anonymous referee.

## References

[1] See, for example the talk by N.J.C. Spooner at the School and Workshop on Neutrino Particle Astrophysics, Les Houches, France, 21 January–1 February 2002. http://leshouches.in2p3.fr.

[2] H. Wulandari et al., in: N.J.C. Spooner, V. Kudryavtsev (Eds.), Proceedings of 4th International Workshop on the Identification of Dark Matter, York, UK, 2–6 September 2002, World Scientific, Singapore, 2003, p. 464.

[3] G. Chardin, G. Gerbier, in: N.J.C. Spooner, V. Kudryavtsev (Eds.), Proceedings of 4th International Workshop on the Identification of Dark Matter, York, UK, 2–6 September, 2002, World Scientific, Singapore, 2003, p. 470.

[4] N.J.C. Spooner (for the UKDM and Boulby Collaborations), in: Y. Suzuki et al. (Eds.), Proceedings of the International Workshop on Technique and Application of Xenon Detectors, Kashiwa, Japan, 3–4 December 2001, World Scientific, River Edge, USA, 2002, p. 68.

[5] E. Aprile et al., in: Y. Suzuki et al. (Eds.), Proceedings of the International Workshop on Technique and Application of Xenon Detectors, Kashiwa, Japan, 3–4 December 2001, World Scientific, River Edge, USA, 2002, p. 165.

[6] M. Yamashita et al., in: Y. Suzuki et al. (Eds.), Proceedings of the International Workshop on Technique and Application of Xenon Detectors, Kashiwa, Japan, 3–4 December 2001, World Scientific, River Edge, USA, 2002, p. 136.

[7] K. Wamba (for the EXO COllaboration), in: D. Su, P. Burchat (Ed.), Proceedings of the 22nd Physics in Collision Conference, Stanford, California, 20–22 June 2002, 2003, p. 343. hep-ph/0210186.
[8] W.B. Wilson et al., SOURCES-4A, Technical Report LA-13639-MS, Los Alamos, 1999.
[9] B.E. Watt, Phys. Rev. 87 (1952) 1037.
[10] V. Chazal et al., Astropart. Phys. 9 (1998) 163.
[11] E.B. Norman et al., Nucl. Phys. A. 390 (1982) 561.
[12] A.J. Howard et al., Astrophys. J. 188 (1974) 131.
[13] http://www-nds.iaea.org/.
[14] S. Agostinelli et al., Nucl. Instrum. Methods Phys. Res. A 506 (2003) 250, see also the GEANT4 web-page at CERN: http://geant4.web.cern.ch/geant4.
[15] D.P. Snowden-Ifft et al., Nucl. Instrum. Methods Phys. Res. A 498 (2003) 155;
T.B. Lawson, for the DRIFT Collaboration, in: N.J. Spooner, V. Kudryatsev (Eds.), Proceedings of the 4th International Workshop on the Identification of Dark Matter, York, UK, 2–6 September 2002. World Scientific, Singapore, 2003, p. 338.
[16] J.F. Briesmeister (Ed.), MCNP-4B, Technical Report LA-12625-M, Los Alamos, 1997.
[17] V.A. Kudryavtsev et al., in: N.J.C. Spooner, V. Kudryavtsev (Eds.), Proceedings of 4th International Workshop on the Identification of Dark Matter, York, UK, 2–6 September 2002, World Scientific, Singapore, 2003, p. 477.
[18] D. Akimov et al., Phys. Lett. B 524 (2002) 245.
[19] http://hepwww.rl.ac.uk/ukdmc/Radioactivity/Index.html.
[20] H.J. Kim et al., Astropart. Phys. 20 (2004) 549.
[21] P. Belli et al., Nuovo Cimento A 101 (1989) 959.
[22] F. Arneodo et al., Nuovo Cimento A 112 (1999) 819.
[23] V.A. Kudryavtsev et al., Astropart. Phys. 17 (2002) 401.
[24] G. Gerbier et al., Astropart. Phys. 11 (1999) 287.
[25] Y.-F. Wang et al., Phys. Rev. D 64 (2001) 013012.
[26] A. Fassò, A. Ferrari, P.R. Sala, in: A. Kling, F. Barao, M. Nakagawa, L. Tavora, P. Vaz (Eds.), Proceedings of the MonteCarlo 2000 Conference, Lisbon, 23–26 October 2000, Springer-Verlag, Berlin, 2001, p. 159;
A. Fassò, A. Ferrari, J. Ranft, P.R. Sala, in: A. Kling, F. Barao, M. Nakagawa, L. Tavora, P. Vaz (Eds.), Proceedings of the MonteCarlo 2000 Conference, Lisbon, 23–26 October 2000, Springer-Verlag, Berlin, 2001, p. 995.
[27] V.A. Kudryavtsev, N.J.C. Spooner, J.E. McMillan, Nucl. Instrum. Methods Phys. Res. A 505 (2003) 688.
[28] M. Robinson et al., Nucl. Instrum. Methods Phys. Res. A 511 (2003) 347.
[29] T.K. Gaisser, Cosmic Rays and Particle Physics, Cambridge University Press, 1990.
[30] M. Aglietta et al. (LVD Collaboration), Phys. Rev. D 58 (1998) 092005;
Phys. Rev. D 60 (1999) 112001.
[31] R.M. McAlpine, Electron Tubes Ltd. Private communications, see also http://www.electron-tubes.co.uk/.
[32] Hamamatsu Photonics KK Ltd., private communication; see also talk by M. Nakahata for the XMASS Collaboration at LowNu2003 Workshop, http://cdfinfo.in2p3.fr/LowNu2003/.
[33] J. Boger et al., Nucl. Instrum. Methods Phys. Res. A 449 (2000) 172.
[34] F. Sauli et al., Nucl. Instrum. Methods Phys. Res. A 386 (1997) 531.
[35] Y. Giomataris et al., Nucl. Instrum. Methods Phys. Res. A 376 (1996) 29.
[36] A. Buzulutskov et al., IEEE Trans. on Nucl. Sci. 50 (2003) 2491.
[37] B. Morgan for the DRIFT and UK Dark Matter Collaborations, Nucl. Instrum. Methods Phys. Res. A 513 (2003) 226.
[38] See, for example, http://pdg.lbl.gov and references therein; see also G.J. Feldman, R.D. Cousins, Phys. Rev. D 57 (1998) 3873.
[39] D. Abrams et al., Phys. Rev. D 66 (2002) 122003.
[40] A.St.J. Murphy, P.F. Smith, D.P. Snowden-Ifft, in: N.J.C. Spooner, V. Kudryavtsev (Eds.), Proceedings of 4th International Workshop on the Identification of Dark Matter, York, UK, 2–6 September 2002, World Scientific, Singapore, 2003, p. 446.
[41] See, for example, the talk by N.J.T. Smith at IDM2002, York, UK, 2–6 September 2002. http://www.shef.ac.uk/~phys/idm2002/talks/.
[42] J.D. Lewin, P.F. Smith, Astropart. Phys. 6 (1996) 87.
[43] See, for example, the talk by N. J. T. Smith at TAUP 2003, Seattle, USA, 5–9 September 2003. http://mocha.phys.washington.edu/~int_talk/WorkShops/TAUP03/Parallel/.